CoFe granules focus coordinated glycolytic mRNA localization and translation to fuel glucose fermentation

Fabian Morales-Polanco[1,2,§], Christian Bates[1,§], Jennifer Lui[1], Joseph Casson[1], Clara A. Solari[3], Mariavittoria Pizzinga[1,4], Gabriela Forte[1], Claire Griffin[1], Paula Portela[3], Mark P. Ashe[1]

[1]Division of Molecular and Cellular Function, School of Biological Sciences, Faculty of Biology, Medicine and Health, The University of Manchester, Manchester Academic Health Science Centre, Michael Smith Building, Oxford Rd., Manchester. M13 9PT. UK

[2]Current Address: Department of Biological Sciences, Stanford University, Clark Center E200, 318 Campus Drive, Stanford, CA 94305

[3]Departamento de Química Biológica, Facultad de Ciencias Exactas y Naturales, Universidad de Buenos Aires, Buenos Aires, Argentina. IQUIBICEN-CONICET

[4]Current Address: MRC Toxicology Unit, Hodgkin Building, PO Box 138, University of Leicester, Lancaster Road, Leicester. LE1 9HN. UK

§ These authors contributed equally to this paper

* corresponding author
e-mail: mark.p.ashe@manchester.ac.uk
phone: +44 (0)161 306 4164

Abstract

Glycolysis represents the fundamental metabolic pathway for glucose catabolism across biology, and glycolytic enzymes are amongst the most abundant proteins in cells. Their expression at such levels provides a particular challenge. Here we demonstrate that the glycolytic mRNAs are localized to granules in yeast and human cells. Detailed live cell and smFISH studies in yeast show that the mRNAs are actively translated in granules, and this translation appears critical for the localization. Furthermore, this arrangement is likely to facilitate the higher level organisation and control of the glycolytic pathway. Indeed, the degree of fermentation required by cells seems intrinsically connected to the extent of mRNA localization to granules. On this basis, we have termed the granules, Core Fermentation (CoFe) granules. Therefore, glycolytic mRNA granules likely represent a conserved means to maintain high-level co-ordinated enzyme synthesis for a critical metabolic pathway.

Introduction

The glycolytic pathway lies at the core of metabolic activity as a virtually ubiquitous biochemical pathway across living cells. The pathway serves both to supply energy and maintain levels of biochemical intermediates (Bar-Even et al., 2012; Nelson and Cox, 2017). Multiple genes express a variety of isoforms for many glycolytic enzymes providing abundant scope for adaptable regulation (Masters et al., 1987; Oparina et al., 2013; Postmus et al., 2012; Warmoes and Locasale, 2014). The pathway was gradually pieced together by a succession of influential biochemists including Meyerhof, Embden, and Parnas (Bar-Even et al., 2012; Barnett, 2005; Schurr and Gozal, 2015). After these major biochemical breakthroughs, interest in central metabolism waned over a period where it was often perceived to perform mundane 'housekeeping' functions (Bar-Even et al., 2012; Ray, 2010). More recently, the pathway and its regulation have received increased interest for various reasons: including connections to cancer and cellular proliferation (Diaz-Ruiz et al., 2011; Gill et al., 2016), moonlighting activities of the glycolytic enzymes in disparate processes (Castello et al., 2015; Kim and Dang, 2005) and renewed interest in central metabolism as a focus for metabolic engineering in a synthetic biology era (Lim and Jung, 2017).

In many aerobic cells, the pyruvate produced by glycolysis is transported and oxidised in the mitochondria via respiration (Nelson et al.). However, under anaerobic conditions and in various aerobic cells, such as yeast, lymphocytes and cancer cells, glucose is fermented through to ethanol or lactic acid; leaving glycolysis as the major source of ATP and intermediates (Lunt and Vander Heiden, 2011). Indeed, the reduction of pyruvate to ethanol or lactic acid can be viewed as an extension of glycolysis.

Given the critical nature of the glycolytic pathway to energy production and cellular metabolism, it is unsurprising to find that the pathway is regulated via a myriad of different mechanisms. These include direct regulation of the enzymes via substrate and product concentration (Wegner et al., 2015), allosteric enzyme regulation via small molecules (Shen et al., 2016) and post-translational covalent modifications (Shenton and Grant, 2003; Tripodi et al., 2015). Aside from controls

of enzymatic activity, other regulatory mechanisms have been described at the level of gene transcription (Chambers et al., 1995; Yeung et al., 2008), mRNA processing/ stability (Krieger and Ernst, 1994; Lunghi et al., 2015), protein stability (Benanti et al., 2007; Lu et al., 2014; Riera et al., 2003) and translation (Daran-Lapujade et al., 2007; Man and Pilpel, 2007). While clearly the glycolytic enzymes and the mRNAs that encode them *can* be regulated, they are often viewed as providing 'housekeeping' functions. Indeed in yeast many of the glycolytic mRNAs are amongst the most abundant, heavily translated mRNAs in the cell. This raises obvious questions about how this level of gene expression is attained both at the transcriptional and post-transcriptional levels? Furthermore, how is this scale of gene expression co-ordinated across the pathway such that appropriate levels of enzyme are produced to generate a metabolic flux that is pertinent to the cellular conditions?

A number of recent observations have supplemented understanding of glycolysis and the role of glycolytic enzymes in cells. For instance, it has become evident that a number of glycolytic enzymes 'moonlight' as RNA binding proteins (Castello et al., 2015). Indeed it has been suggested that many of the glycolytic proteins bind to glycolytic mRNAs to co-ordinate control of the pathway (Matia-Gonzalez et al., 2015). In addition, the localization of two glycolytic mRNAs in yeast, *PDC1* and *ENO2,* has been identified as important in their translation control and in the formation of mRNA processing bodies after glucose starvation (Lui et al., 2014).

mRNA localization has been commonly considered as a means to generate localized sources of protein, with specific examples involved in cellular polarization identified across many biological systems- *ASH1* mRNA in yeast (Long et al., 1997), *bicoid* in *Drosphila* oocytes (Berleth et al., 1988) and *Vg1* in *Xenopus* oocytes (Melton, 1987). In these cases, translation of the mRNA is repressed during transit: a process requiring motor proteins and cytoskeletal elements (Besse and Ephrussi, 2008). Another situation where translationally repressed mRNAs become localized is under stress conditions, where non-translated mRNAs can enter either mRNA processing bodies (P-bodies) or stress granules to play roles in mRNA degradation and/or storage (Hoyle and Ashe,

2008; Hubstenberger et al., 2017; Jain and Parker, 2013). More global assessments of mRNA localization suggest that the phenomena is widespread: large numbers of mRNA species are localized in *Drosophila*, neuronal cells and yeast (Lecuyer et al., 2007),(Gadir et al., 2011; Miyashiro et al., 1994; Pizzinga and Ashe, 2014; Zipor et al., 2009; Zivraj et al., 2010). Even so, mRNA localization is rarely thought to play a role in core housekeeping functions such as central metabolism.

In this study, we show that glycolytic mRNAs in yeast and human cells are specifically localized to granules. In yeast, we define the Core Fermentation (CoFe) granule, a core glycolytic mRNA granule where glycolytic mRNAs are co-ordinately colocalized. We show that localized mRNAs are translated in these granules and that their translation is a prerequisite for the mRNA to be localized. Finally, we show that the presence of mRNA granules correlates with the degree of glycolytic function required by the cell. We suggest that the localization of these mRNAs provides a means to co-ordinately generate the scale of protein expression required for such a critical pathway.

Results

Most glycolytic mRNAs localize to granules under active growth conditions

Previous work from our laboratory has highlighted that the glycolytic mRNAs, *PDC1* and *ENO2*, encoding pyruvate decarboxylase and enolase, respectively, are translated in cytoplasmic granules (Lui et al., 2014) (Figure 1A). An obvious question arising from this work is whether glycolytic mRNAs are generally translated as part of translation factories i.e. are other glycolytic mRNAs similarly localized? To evaluate this in live cells, we made use of the m-TAG system, which borrows elements from the MS2 bacteriophage to essentially tether GFP to mRNA (Haim-Vilmovsky and Gerst, 2011). Accordingly, MS2 stem loops were directly inserted into the 3'UTR sequences of the glycolytic genes at their endogenous genomic loci. The localization of the resulting mRNAs was then followed via co-expression of the MS2 coat protein-GFP fusion (MS2-CP-GFP). It should be noted that MS2-CP-GFP expression in isolation generates diffuse fluorescence throughout the cytosol (Figure 1B). In contrast, when MS2 stem loops are integrated into glycolytic mRNA 3'UTR sequences, the vast majority of the resulting mRNAs are observed in granules, including the hexokinase mRNAs *GLK1*, *HXK1* and *HXK2*; the phosphoglucose isomerase mRNA, *PGI1*; the phosphofructokinase mRNAs, *PFK1* and *PFK2*; the fructose-bisphosphate aldolase mRNA, *FBA1*; the triose phosphate isomerase enzyme, *TPI1*; the glyceraldehyde 3-phosphate dehydrogenase mRNA, *TDH3*; the phosphoglycerate kinase, *PGK1*; 3phosphoglycerate mutase mRNA, *GPM1*; the enolase mRNA, *ENO1*; the pyruvate kinase mRNA, *CDC19*; and the major alcohol dehydrogenase mRNA, *ADH1* (Figure 1C and D). Notably, not all MS2-tagged mRNAs localize to granules of this kind (Lui et al., 2014; Simpson et al., 2014), for instance, two non-glycolytic mRNAs, *GLO1* and *PFK26*, where the gene products are involved in the control of the glycolytic pathway, and the glycolytic mRNA, *PYK2*, are not observed in granules (Figure 1B).

Recent commentaries have highlighted that caution needs to be applied to the interpretation of mRNA localization using MS2-based technology due to a potential for the accumulation of fragments of mRNA carrying the MS2 stem loops (Garcia and Parker, 2015, 2016; Haimovich et al., 2016; Heinrich et al., 2017). It is possible that such fragments would accumulate at sites of mRNA degradation. To

directly assess whether this is the case for the granules observed here in actively growing cells, a range of approaches were taken.

Firstly, it should be noted that all of the experiments presented are conducted on cells actively growing in nutrient replete media. Under these conditions in our experiments, P-bodies are largely absent (Lui et al., 2014), so the accumulation of mRNA fragments at sites of mRNA decay seems unlikely. Secondly, the introduction of MS2 stem loops directly into the yeast genome within the 3'UTR sequence of the relevant gene has little impact on the steady state level of the mRNAs (Figure S1A). The exception is *PGK1* where, as previously shown, the level of this mRNA is reduced in the presence of MS2 stem loops (Simpson et al., 2014). Thirdly, any stabilising impact of MS2 stem loops in the 3'UTR of an mRNA should be overcome by reducing the number of MS2 stem loops. In our system 12 stem loops are present, when this number is reduced to 5 stem loops for the *PFK2* and *ENO1* mRNAs, mRNA granules were still evident in cells (Figure S1B). Fourthly, in terms of MS2 stem loops generating stable degradation products of MS2 containing mRNAs, the major mRNA species observed on Northern blots under active growth conditions for either the non-tagged or MS2-tagged *ENO2* and *PDC1* mRNAs were the full-length mRNAs (Figure S1C). However, under conditions where P-bodies are obvious, such as after glucose depletion, degradation fragments were much more evident for MS2-tagged mRNAs than non-tagged (Figure S1C). Finally, a single molecule fluorescent in situ hybrdization (smFISH) strategy where probes were targeted to either the MS2 stem loops or the body of the mRNA revealed greater than 75% signal overlap between these two probes (Figure 1E and F). This result suggests that the MS2 region of the mRNA reports the localization of full length mRNAs. In addition, significant overlap is seen between the MS2-CP-GFP protein signal and either the MS2 probe signal or mRNA body probe signal. Although, as the m-TAG system used here is not a single molecule technique the MS2-CP-GFP signal is only seen for those granules that exceed a specific intensity threshold in the smFISH channels (Figure 1F)(Pizzinga et al., 2019). Overall, the combination of different validatory analyses used show that stable MS2 fragments are unlikely to represent a specific issue in our experiments.

However, it is still plausible that insertion of MS2 stem loops could alter some aspect of an MS2-tagged mRNAs fate. Therefore, in order to provide an independent assessment of the localization of endogenous glycolytic mRNAs further smFISH experiments were conducted. smFISH strategies commonly use ~30-50 fluorescently labelled oligonucleotides which are hybridized to mRNAs in fixed cells (Pizzinga et al., 2019; Tsanov et al., 2016). Since many glycolytic genes are present in yeast as multiple paralogues with high levels of sequence identity, the use of smFISH to unambiguously study the localization of individual mRNA species can prove problematic. Therefore, sets of smFISH probes were designed to study the localization of mRNAs encoded by glycolytic genes that either lack paralogues or harbor substantial sequence differences to their paralogues. As a result four different glycolytic mRNAs, *GPM1*, *FBA1*, *TPI1* and *PGK1* were analyzed and shown to localize specifically to granules (Figure 2A). In terms of the number of granules per cell the smFISH data on endogenous mRNAs are entirely complementary to the live cell MS2-tagged mRNAs (*cf*. Figure 2B and 1D). One of the key advantages of our smFISH versus the m-TAG experiments is that for the smFISH data, single mRNAs are visible. This allows an estimate of mRNA copy number per cell and the proportion of single mRNAs present in multi-mRNA granules (Pizzinga et al., 2019). From these data, it is clear that over ~60-70% of specific glycolytic mRNAs are present in large granules (Figure 2C). These results correlate well with live cell m-TAG data, where a similar fraction of the *PDC1* and *ENO2* mRNAs were found in granules (Lui et al., 2014). Overall the data confirm that glycolytic mRNAs are housed in large cytoplasmic bodies or granules, and combined with our concurrent studies on translation factor mRNAs (Pizzinga et al., 2019), indicate that the localization observed with the MS2 system in actively growing cells can be representative and meaningful to the localization observed for an untagged mRNA.

Glycolytic mRNAs colocalize to the same RNA granules

Our previous assessment of the *ENO2* and *PDC1* mRNAs suggested that these mRNAs colocalize to the same granules, but are distinct from translation factor mRNA granules (Lui et al., 2014; Pizzinga et al., 2019). On this basis, we speculated that the colocalization of glycolytic mRNAs might generally allow a concerted

production and/or regulation of the pathway enzymes. More recent work highlights the potential for co-translational assembly of components of the glycolytic pathway (Shiber et al., 2018), which again hints that actively translating glycolytic mRNAs might colocalize. In both the live cell and fixed cell mRNA localization experiments presented here, both the pattern and number of mRNA granules in a cell is remarkably similar across the different glycolytic mRNAs (cf. Figure 1C and 2A; cf Figure 1D and 2B). This similarity is consistent with a model where many of the glycolytic mRNAs colocalize to the same site.

However, in order to directly assess glycolytic mRNA colocalization, we made use of a PP7/ MS2 colocalization system, which allows the simultaneous visualization of two mRNAs in the same live cell (Hocine et al., 2013; Lui et al., 2014; Pizzinga et al., 2019). More specifically, a series of yeast strains were generated carrying PP7-tagged *ENO2* mRNA as well as another MS2-tagged glycolytic mRNA. By co-expressing the MS2 and PP7 coat proteins fused to mCherry and GFP respectively, the localization of each MS2-tagged mRNA could be compared directly to that of *ENO2* mRNA in the same living cell. As previously shown (Lui et al., 2014), we observed a strong colocalization of *PDC1* with *ENO2* using this system (Figure 3A). Equally, for many of the glycolytic enzymes tested, a high degree of colocalization with the *ENO2* mRNA pattern was observed (Figure 3B).

In order to provide corroboration for the colocalization observed in live cells using the PP7/ MS2 systems, we assessed pairwise colocalization of endogenous unmodified glycolytic mRNAs using smFISH (Figure 4A). In order to objectively measure colocalization a computational strategy was developed. In short, the distance between the centroid of the granules for one mRNA was measured relative to the centroid of the nearest neighbouring granule for the other mRNA (Figure 4B). Given that the average diameter of a multi-RNA granule is ~450nm, in the order of 80-90% of RNA granules are deemed to overlap with each other - as their centroids are less than 200nm apart (Figure 4C). Since each mRNA is present in ~20 multi-mRNA foci and a similar number of single mRNA foci, we were concerned that a high level of colocalization might be apparent simply due to the proportion of cytosolic space occupied by the mRNA foci. Therefore, we

established a simulation analysis where the position of simulated foci was randomized within the cell and cross-compared with randomized simulated foci from a second mRNA. From this analysis, it is clear that relative to this simulated control the various tested glycolytic mRNAs display evidence for significant colocalization (Figure 4C). Overall, these results and the experiments in live cells suggest that there is a genuine colocalization of glycolytic mRNAs to multi-mRNA granules in yeast cells growing under optimal growth conditions. These mRNAs encode enzymes that catalyse most of the reactions that are required for the fermentation of glucose to ethanol in yeast; therefore we have termed the granules that house these mRNAs, 'Core Fermentation' mRNA granules or CoFe granules.

mRNA translation both occurs in and is required for localization to CoFe granules

Previously, we have shown that in contrast to most mRNA containing granules, which carry translationally repressed mRNAs, the granules housing the glycolytic mRNAs *PDC1* and *ENO2* are sites where these mRNAs are translated (Lui et al., 2014). A variety of experiments support this hypothesis, including data from a FRAP assay, the quantification of ribosome associated mRNA relative to granule associated mRNA and the use of drugs that inhibit translation. To extend this analysis further, a technique called TRICK (translating RNA imaging by coat protein knockoff) was used, which allows visualization of translation in live cells (Halstead et al., 2015; Pizzinga et al., 2019). This technique relies upon observations that a PP7 coat protein fusion bound to PP7 stem loops upstream of the STOP codon is displaced under active translation conditions, whereas the MS2 coat protein fusion tethered downstream of the STOP codon remains associated (Halstead et al., 2015) (Figure 5A). For *PDC1* mRNA under active growth conditions, most granules observed only carry the MS2-CP-mCherry (MS2-CP-mCh) fusion protein (Figure 5B and C). In contrast, after a 10 minutes glucose depletion to elicit a robust and global inhibition of protein synthesis (Ashe et al., 2000), both MS2-CP-mCh and PP7-CP-GFP colocalize to granules (Figure 5B and C). This result supports our previous work showing that under active growth conditions the glycolytic mRNAs such as *PDC1* and *ENO1* are translated in granules,

and combined with the colocalization studies, suggest that the CoFe granules serves as a translation factory for the production of glycolytic enzymes.

Another key question is whether translation of a molecule of mRNA is a requirement for entry to the granule. In order to address this question, we selected the *PDC1* mRNA and sought to limit its translation then assess the impact on localization. More specifically, we adopted two different strategies toward reducing *PDC1* mRNA translation. In the first approach a STOP codon was inserted immediately downstream of the translation START codon (*PDC1-sc*) (Figure 5D). We reasoned that this would severely reduce the number of ribosomes associated with this mRNA and significantly increase the pool of non-translated *PDC1* mRNA. As a second strategy, a stem loop was inserted into the *PDC1* mRNA 5'UTR, upstream of the START codon (*PDC1-sl*) (Figure 5D). Introduction of this well-characterized stem loop (ΔG value of −41 kcal/mol) has previously been shown to reduce translation of specific mRNAs by limiting scanning of the 43S preinitiation complex through to the AUG Start codon (Palam et al., 2011; Pizzinga et al., 2019; Vattem and Wek, 2004). In strains carrying these altered *PDC1* mRNAs, mRNA localization was followed relative to the non-modified mRNA using the MS2 system.

Introduction of either the STOP codon or the stem loop structure into the PDC1 mRNA dramatically reduced the number of *PDC1-MS2* mRNA granules: decreasing from ~20 granules per cell to less than 5 (Figure 5E, F and G). Coincident with this effect on the number of mRNA granules in the cell, both strategies used to limit *PDC1* mRNA translation also lead to reduced mRNA levels (Figure 5H). Insertion of the STOP codon caused an ~8-fold reduction in *PDC1-MS2* mRNA, whereas stem loop insertion reduced mRNA levels ~2-fold. The reduction of mRNA caused by the introduction of the STOP codon is consistent with premature STOP codon mRNAs leading to nonsense mediated mRNA decay (Hagan et al., 1995). The impact of the stem loop on *PDC1* mRNA levels is not as pronounced as the STOP codon insertion, and it is a little surprising that this insertion leads to mRNA destabilisation, as this same stem loop has been inserted into a number of mRNAs without impacting upon overall mRNA levels (Palam et al., 2011; Pizzinga et al.,

2019; Vattem and Wek, 2004). However, this result does highlight the intimate connection between the translation of an mRNA and its stability, and adds to many observations showing that a reduction in translation can lead to mRNA destabilization (Roy and Jacobson, 2013).

A surprising observation was made when the localization of the P-body marker Dcp2p was assessed in cells bearing either the *PDC1-sc* or *PDC1-sl* mRNAs. In both strains, Dcp2p was constitutively present in P-bodies even in unstressed cells, and the *PDC1-sc* and *PDC1-sl* mRNAs colocalized with these bodies (Figure 5B). This result is especially intriguing as generally P-bodies are barely visible unless cells are stressed in some way (Lui et al., 2014), yet in these unstressed cells just a single point mutation to introduce a STOP codon is sufficient to induce P-body formation. This result is also interesting with regard to the controversy surrounding MS2-tagging. The specific introduction of a mutation that inhibits translation to destabilize an mRNA changes the pattern dramatically and causes P-body formation. Therefore, if the RNA granules observed for non-mutated glycolytic mRNAs during exponential growth (Figure 1C) were due to the accumulation of RNA fragments carrying the MS2 stem loops, we would expect a similar colocalization with P-body markers. However, we do not observe such colocalization with P-body markers in unstressed cells (Lui et al., 2014; Pizzinga et al., 2019).

Overall, these results highlight that in keeping with many observations over the years it is difficult to alter the translation of an mRNA without affecting its stability (Mugridge et al., 2018; Roy and Jacobson, 2013). However, the results do suggest that as well as translation occurring in the glycolytic mRNA granules, translation is important for mRNAs to enter these granules, since when translation is reduced alternative mRNA fates such as degradation and relocalization to P-bodies become apparent.

Glycolytic mRNA localization varies according to the level of fermentation

In order to understand the potential physiological role these granules play, a series of experiments were undertaken growing yeast on a range of carbon

sources selected based upon the pathways required for carbon source metabolism. For example, while yeast cells ferment glucose to ethanol even under aerobic conditions, for other carbon sources the degree of fermentation varies. Yeast cells grown on ethanol as the sole carbon source, derive their energy from respiration and only require the glycolytic enzymes for gluconeogenesis. Raffinose is catabolised initially via the expression of the secreted enzymes invertase (Suc2p) and α-galactosidase (Mel1p). These enzymes yield the monosaccharides glucose, fructose and galactose, which are readily available for fermentation via the glycolytic enzymes (Barnett, 1976). Equally yeast that are pre-adapted to galactose, express enzymes of the Leloir pathway allowing fermentation of this sugar via entry into the glycolytic pathway (Timson, 2007).

Microscopic analysis revealed that yeast cells grown on glucose, raffinose or galactose harboured approximately 10-20 granules of either *PDC1* mRNA or *ENO1* mRNA per cell, whereas cells grown on ethanol harboured significantly fewer granules (Figure 6A and B). In terms of *PDC1* and *ENO1* mRNA levels, these also vary with carbon source. Consistent with glucose representing the preferred yeast carbon source, for both mRNAs, glucose grown cells harbour significantly more mRNA than cells grown on most other carbon sources. Therefore, these results show that both the level of glycolytic mRNAs and prevalence of CoFe granules vary depending on the carbon sources. In particular, the presence of CoFe granules appears to correlate with a requirement for glycolytic flux to utilise the provided carbon source. In contrast, the overall level of the mRNA is more tied to the quality of the carbon source rather than the pathway required for its utilization.
Overall, the data are consistent with a view that the localization of glycolytic mRNAs to CoFe granules represents a strategy allowing high-level co-ordinated production of glycolytic enzymes in translation factories.

Glycolytic mRNA granules are also evident in human cells

In order to assess whether a similar organization of glycolytic mRNAs might exist in higher eukaryotic cells, smFISH analysis was conducted for four different glycolytic mRNAs in HeLa cells, two enolase mRNAs (*ENO1* and *ENO2*), lactate dehygrogenase mRNA (*LDHA)* and a phosophofructokinase mRNA (*PFKM)*. For all

four of the selected mRNAs, variation in mRNA signal was observed both in terms of particle size and intensity (Figure 7A, data not shown). In particular large intense mRNA foci were observed suggesting that granules harbouring multiple mRNAs can also be a feature of higher eukaryotic cells. Similar observations were made in other cell lines such as HFF-1 cells and SH-SY5Y cells (data not shown). This opens up the possibility that glycolytic mRNAs might be co-ordinately localized in higher cells. Therefore, a multichannel smFISH approach was taken. Here, evidence for a specific colocalization of the *ENO2* and *PFKM* mRNAs was obtained (Figure 7B and C). While the degree of colocalization is not as comprehensive as observed in yeast, these data do show that in actively growing human tissue culture cells, glycolytic mRNAs can be localized to granules, and that these granules can contain more than one type of glycolytic mRNA.

Discussion

mRNA localization serves critical functions in the expression of proteins at specific loci within cells and in the response to stress in terms of P-body and stress granule formation (Pizzinga and Ashe, 2014). In this study, we suggest that mRNA localization to CoFe granules can co-ordinate whole pathways of metabolism. We use a combination of live cell experiments and smFISH to show that glycolytic mRNAs localize to granules in yeast and human cells. In stark contrast to mRNAs localizing to P-bodies, stress granules or transport granules, in yeast the glycolytic mRNAs are translated in CoFe granules, and their translation is a requirement for localization.

Recent evidence suggests that liquid-liquid phase separation (LLPS) within cells produces membraneless compartments where enzymatic reactions and processes can occur. For instance, in nucleoli rRNA is produced via numerous complex reactions (Brangwynne et al., 2011), while in the centrosome microtubule nucleation occurs (Zwicker et al., 2014). The CoFe granules described here conform to many of the properties of phase-separated condensates: they are dynamic, can be observed to fuse and are disrupted by low concentrations of 1,6-hexanediol. Therefore, our data suggest that translated glycolytic mRNAs are present in such phase separated bodies where enzymatic activity is not only maintained but might actually be enhanced (Kojima and Takayama, 2018).

Enhanced translation of mRNA is therefore one possible explanation as to why the glycolytic mRNAs would be localized within granules. Previous observations from our lab have shown that up to 95% of the glycolytic mRNAs are translated (Lui et al., 2014). In addition, the glycolytic mRNAs are amongst the most abundant in the cell and so may require rather specific mechanisms to maintain their high rates of translation. Equally LLPS has previously been associated with altered efficiency of a host of biological processes and enzymes (Zhou et al., 2008), so translation may prove to represent another example of such a process.

Another possible rationale for localized mRNA translation is to aid the formation of multi-protein complexes. Many of the glycolytic enzymes are present in

multimeric complexes. For example almost all of the glycolytic enzymes function as multimers: in yeast the phosphofructokinase enzyme is present as an octamer (Schwock et al., 2004), phosphoglycerate mutase and pyruvate kinase are tetramers (Jurica et al., 1998; Rigden et al., 1998) whereas enolase is dimeric (Sims et al., 2006). Co-translation of individual mRNAs at the same site within cells could therefore aid the formation and productive folding pathways for these complexes. A range of precedents exist for the co-translational production of complexes across various biological systems (Halbach et al., 2009; Kamenova et al., 2019; Shiber et al., 2018; Wells et al., 2015), while a systematic analysis in *Schizosaccharomyces pombe* suggests that co-translational production of protein complexes is widespread with a substantial fraction of proteins co-purifying with mRNAs that encode interacting proteins (Duncan and Mata, 2011). Notably, in recent work characterizing several different protein complexes in yeast and the propensity for co-translational folding, the *PFK1* and *PFK2* phosphofructokinase mRNAs were identified as key examples where the translated products are co-translationally assembled or folded (Shiber et al., 2018).

It has also been shown that as well as forming multimeric single enzyme complexes, various different glycolytic enzymes can be compartmentalized into much larger complexes (Masters, 1991). A variety of observations suggest that the physical compartmentalization of glycolysis is advantageous. For instance, in protozoan organisms such as *Trypanosoma* and *Leishmania*, a specific membrane-bound organelle called the glycosome has evolved, which is devoted to efficient glycolytic activity (Haanstra et al., 2016). Furthermore, in human cells, such as skeletal muscle cells, neurons and erythrocytes; glycolytic enzymes can be organized as complexes co-ordinated either on membranes or the cytoskeleton (Knull and Walsh, 1992; Puchulu-Campanella et al., 2013). Moreover, a glycolytic metabolon has also been described in yeast (Masters, 1991) and it is stabilized by various weak interactions with actin (Araiza-Olivera et al., 2013). These multi-enzyme complexes are likely to promote both the channelling of metabolites from one enzyme to the next, as well as the reduction of potentially toxic intermediates. More recent work in yeast has shown that while glycolytic enzymes are broadly cytosolic under non-stress conditions, they can coalesce into 'G-bodies' in

response to hypoxic stress (Jin et al., 2017). Overall, therefore the co-production of the glycolytic enzymes at the same site by virtue of co-ordinated mRNA localization could promote the co-translational formation of some of these higher order complexes of enzymes. Although it should be noted that our own data suggest that under active growth conditions fluorescent-protein tagged forms of the enzymes are generally found throughout the cytosol (Lui et al., 2014).

Another point worth reflecting upon when considering the role of the CoFe granules is that several glycolytic enzymes have extra glycolytic or 'moonlighting' functions outside of their role in glycolysis. For example, many of the glycolytic enzymes have been identified as RNA binding proteins that appear to interact with their own mRNA (Castello et al., 2015; Matia-Gonzalez et al., 2015). In addition, yeast enolase is important for both the mitochondrial import of $tRNA^{Lys}_{CUU}$ (Entelis et al., 2006) and for vacuole fusion (Decker and Wickner, 2006), and yeast fructose-1,6-bisphosphate aldolase is important for vacuolar H+-ATPase function (Lu et al., 2007). Many further moonlighting functions of glycolytic enzymes, including nuclear functions in transcription, DNA replication/ repair and histone modification have been described (Boukouris et al., 2016). One possible explanation for the presence of CoFe granules could be that they serve as a focus for the co-ordinated high-level production of the glycolytic machinery *en masse*, whereas individual translated glycolytic mRNAs outside of this factory could provide the capacity for moonlighting protein production.

In summary, glycolysis is perhaps the most fundamental of all biological pathways. The enzymes of the pathway are regulated at almost every level and have evolved distinct functions. The pathology of many disease conditions is intimately connected to the glycolytic pathway. For instance, aerobic glycolysis serves as a hallmark of many malignant cancers and the surrounding stroma, which can serve as a negative prognostic indicator due to increased resistance to therapy (Lee and Yoon, 2015; Ngo et al., 2015). The identification and characterization of granules harbouring translated glycolytic mRNAs can only serve to increase understanding of the functions, regulation and possibility for genetic adjustment of this key metabolic pathway.

Materials and Methods

Yeast growth conditions. Strains used in this study are listed in Table I. Yeast strains were grown in synthetic complete (SC) with 2% glucose at 30°C to exponential phase. Cells were incubated for 30 min in media lacking methionine to induce expression of the pCP-GFP/mCh fusions prior to imaging. For growth on alternative carbon sources SC media was supplemented with 2% raffinose, 2% galactose or 3% ethanol. For stress conditions, cells were incubated in media lacking glucose for 10 minutes.

Yeast strain and plasmid construction. MS2 and PP7 tagged strains were generated as previously described (Haim-Vilmovsky and Gerst, 2011; Hocine et al., 2013), using plasmid reagents generously donated by Jeff Gerst and Robert Singer. Dual MS2 and PP7 tagged strains were generated by crossing the single tagged haploid strains. Subsequent diploid strains were selected, sporulated and the appropriate dual tagged haploid strains were verified by PCR. The strain harbouring a premature stop codon in the *PDC1* ORF was generated via recombination of a mutant PCR product generated from the *PDC1-MS2* tagged strain. More specifically, oligonucleotides with a specific mutation in the upstream primer were used to amplify a *PDC1::HIS5::MS2* cassette from genomic DNA prepared from an intermediate strain in the *PDC1-MS2* m-TAG procedure (Haim-Vilmovsky and Gerst, 2011). The mutation introduces a premature STOP codon in the *PDC1* ORF. The *PDC1::HIS5::MS2* cassette was then transformed and recombined into the *PDC1* locus of the yMK467 strain. Removal of the *HIS5* marker was carried out using a Cre recombinase strategy as previously described (Haim-Vilmovsky and Gerst, 2011). TRICK strains were generated using a similar approach to MS2 or PP7 tagging, but using a DNA template developed for TRICK in yeast (Pizzinga et al., 2019). For generation of the yEPlac195-*PDC1* (p*PDC1-MS2*) plasmid, *PDC1-MS2* was amplified from genomic DNA of yMK1586 and cloned into yEPLac195. A stem loop sequence (Vattem and Wek, 2004) was inserted upstream of the start codon in *PDC1* using Gibson assembly (Gibson et al., 2009) to generate plasmid yEPlac195-PDC1-SL (p*PDC1*-MS2 (sl)).

Single molecule fluorescent *in situ* hybridisation (smFISH). For yeast cultures, smFISH was performed as previously described (Pizzinga et al., 2019). In brief exponential yeast were fixed in 4% EM-grade formaldehyde (15714-S; Electron Microscopy Sciences) for 45 min, then spheroplasted and permeablized with 70% ethanol. Gene-specific 20n antisense oligonucleotides were designed with a 59n Flap sequence, to which fluorescently labelled oligonucleotides were annealed (Pizzinga et al., 2019; Tsanov et al., 2016). The conjugated fluorophores included Alexa Fluor 488, Alexa Fluor 546, ATTO 590 and Alexa Fluor 648. 20 pmol fluorescently labelled smFISH probe was added to the cells in hybridization buffer (10 mg E. coli tRNA, 2 mM Ribonucleoside Vanadyl Complex, 200 µg/ml BSA, 10% dextran sulfate, 10% formamide, and 2× SSC in nuclease-free water). Cells were then washed in 10% formamide and 2× SSC and adhered to 0.01% poly-L-lysine–coated coverslips before mounting in ProLong diamond antifade mounting solution with DAPI (Life Technologies).

For human cell experiments, HeLa cells were seeded in Dulbecco's modified Eagle's medium supplemented with 10% fetal bovine serum onto 13 mm laminin coated coverslips in sterile 24-well plates, then were fixed in methanol for 10 min at -20^{o}C. Fixed cells were washed in 10% Formamide, 2x SSC buffer in nuclease-free water for 30 min at room temperature, then hybridized probes (as above) were added at a concentration of 25 nM for Cy7-conjugated probes and 75 nM for Cy5-conjugated probes at 37^{o}C overnight. Cells were then washed and mounted (Tsanov et al., 2016).

Fluorescent microscopy. All yeast epifluorescent microscopy was performed on a Nikon Eclipse E600 or a Delta Vision microscope (Applied Precision) equipped with a Coolsnap HQ camera (Photometrics), using a 100x/ 1.40 NA oil plan Apo objective. Fluorescent parameters for each fluophore are as follows; GFP (excitation-490/20 nm, emission- 535/50 nm); mCherry (excitation- 572/35 nm, emission-632/60 nm); and CFP (excitation- 436/10 nm, emission- 465/30). For routine live-cell imaging, exponentially growing cells were viewed on poly-L-lysine coated glass slides and images were taken with a *z*-spacing of 0.5µm. Images

were acquired using Softworx 1.1 software (Applied Precision) and processed using Image J software package (National Institute of Health, NIH).
Images of human cells were acquired on an Olympus IX83 inverted microscope using Lumencor LED excitation, a 100x objective and the Penta filter set. The images were collected using a Retiga R6 (Qimaging) CCD camera with a *z*-optical spacing of 0.2 µm. Raw images were then deconvolved using the Huygens Pro software (SVI).

Confocal microscopy. SmFISH images were collected on a Leica TCS SP8 AOBS inverted gSTED microscope using a 100x/1.40 Plan APO objective and 1x confocal zoom, as described previously (Pizzinga et al., 2019). DAPI staining was detected using a photon multiplying tube with a blue diode 405nm laser (5%). Confocal images of smFISH signals were collected using hybrid detectors with the following detection mirror settings; Alexa Fluor 488 410-483nm (5 to 50µs gating); Alexa Fluor 546 556-637nm (5 to 35µs gating); ATTO 590 603-637nm (5 to 35µs gating); Alexa Fluor 647 657-765nm (5-50µs gating) using the 488nm (60%), 550nm (60%), 593nm (60%) and 646nm (60%) excitation laser lines, respectively. Images were collected sequentially in 200nm *z*-sections. Acquired images were subsequently deconvolved and background subtracted using Huygens Professional (Scientific Volume Imaging).

Quantification of microscopy and statistics. For quantification of granule numbers per cell from live cell experiments, 50 cells were counted for each strain. For quantification of overlapping MS2 and PP7 signal in double-tagged strains or TRICK strains, 100- 150 granules were considered for each strain over three biological repeats. GraphPad Prism 6 (GraphPad Software, Inc.) was used to produce the graphs and to calculate the standard deviation, indicated by error bars. Two-way ANOVA was performed using GraphPad Prism 6. * indicates a P value < 0.0001.

smFISH images were processed and analysed using FISH-quant (Mueller et al., 2013) or FindFoci (Herbert et al., 2014) to identify spot position and size and provide spot enhancement via dual Gaussian filtering. Cell outlines were

automatically generated using a modified version of the CellProfiler pipeline provided with FISH-quant. Spot colocalization and other foci characteristics were assessed and quantified using custom scripts in python and R. Colocalization analysis was performed by pairing spots between channels based on spot centroid distance in 3D space (Eliscovich et al., 2017). Spots were deemed to colocalize if the 3D distance between them was less than the summed radius of the two spots. mRNA quantitation was performed using Gaussian fitting, as described previously (Pizzinga et al., 2019). Simulated controls were performed by randomly sub-sampling spot characteristics, such as size in *x*, *y* and *z* planes, and arbitrarily positioning these within a simulated volume, typical of a yeast cell, as measured using the custom CellProfiler pipeline. The colocalization of these randomly positioned foci was subsequently processed using the same script outlined above, and iterated 1000 times per RNA.

Quantitative RT-PCR (qRT-PCR). RNA preparations were carried out using Trizol as described by the manufacturer (Thermofisher scientific), followed by isopropanol precipitation then treatment with Turbo DNase (Thermofisher scientific). qRT-PCR was performed in a two-step manner using a ProtoScript First Strand cDNA synthesis kit (Biorad) and iQ SYBR Green Supermix (BioRad) according to manufacturer's instructions. Reactions were performed using 100ng of cDNA. iTaq Universal SYBR Green One Step Kit (Bio-Rad) was used to carry out one-step qRT-PCR and reactions were performed using 300ng of RNA. A CFx Connect Real-Time system was used to run reactions. Samples were run in triplicate and normalized to *ACT1* mRNA, and the fold change was calculated using either the $2^{-\Delta\Delta Cq}$ or the Pfaffl method (Livak and Schmittgen, 2001; Pfaffl, 2001).

Figure Legends

Figure 1. MS2-tagged glycolytic mRNAs are localized to granules in *S. cerevisiae*. (A), (B) and (C), *z*-stacked images of strains expressing *MS2*-tagged mRNAs as labelled and the MS2 coat protein GFP fusion. Scale bar: 2μm. (D) A dotplot showing the variation in the number of granules per cell for each of the *MS2*-tagged strains above. n=50. The mean ± SD are indicated for each strain. (E) *z*-stacked images of smFISH performed on strains expressing *MS2*-tagged mRNAs and the MS2 coat protein GFP fusion. smFISH was performed for the canonical *GPM1* gene (smGENE) or the *MS2* stem loop sequence (smMS2). Scale bar: 3μm. (F) Beeswarm plot showing the proportion of smMS2 foci that colocalize with smGENE foci for a subset of strains expressing *MS2*-tagged glycolytic mRNAs. Each dot represents a single cell. n>300.

Figure 2. smFISH analysis reveals that endogenous glycolytic mRNAs are present in multi-mRNA granules. (A) Upper cartoon depicts an overview of the smFISH experiment. Multiple probes that are complementary to the mRNA of interest (black) are tagged with a specific fluorophore (red). Lower panels show *z*-stacked images of smFISH experiments performed for a number of endogenous glycolytic mRNAs. Both mRNAs (red) and nuclei (blue) are shown. Dotted line represents the outline of the cell, determined using brightfield micrographs. Scale bar: 3μm. (B) Beeswarm plot showing the number of multi-mRNA (>2.5mRNAs) granules that exist per cell for a number of endogenous mRNAs. Grey box and line represent the interquartile range and the median, respectively, for each mRNA. Each dot represents a single cell. n>300. (C) Beeswarm plot showing the proportion of mRNA that resides within multi-mRNA granules (>2.5mRNAs) per cell. Grey box and line represent the interquartile range and the median, respectively. n>300.

Figure 3. Glycolytic mRNAs colocalize to granules in actively growing cells. (A) and (B). *z*-stacked images showing localization of various *MS2*-tagged mRNAs (via co-expression of the MS2-CP-mCh fusion) relative to the *ENO2-PP7* mRNA (visualized using co-expression of the PP7-CP-GFP fusion). The percentage of

observable tagged mRNA colocalizing with the *PP7*-tagged mRNA is indicated ± SD. Scale bars: 2 μm.

Figure 4. smFISH confirms that glycolytic mRNAs colocalize in granules. (A) *z*-stacked example image of smFISH colocalization experiments. Lower panel represents foci identified after a threshold has been applied using FindFoci (see methods). Scale bar: 3μm. (B) Beeswarm plot showing the proportion of colocalized smFISH foci. Colocalization was assessed in a pairwise manner using smFISH foci identified via Fish-quant (see methods). Simulated colocalization was assessed by sub-sampling foci properties across a number of pairwise comparisons (see methods). Grey box and line represent the interquartile range and the median, respectively. Each data point represents a single cell, n>300. (C) Histogram and density plot showing the binned distance between paired smFISH foci centroids.

Figure 5. mRNAs translation in CoFe granules is required for localization (A) Schematic of TRICK reporter system. Ribosomes on translated RNAs 'knock off' the PP7 coat protein GFP fusion whilst on untranslated RNAs the coat protein remains bound. (B) *z*-stacked images of TRICK tagged mRNAs co-expressing the MS2-CP-mCh fusion and the PP7-CP-GFP fusion, in + and – glucose. Scale bars: 3 μm (C) Quantification of MS2-CP-mCh only granules as a percentage of total granules observed in TRICK tagged mRNAs in + and – glucose conditions. Error bars are ± SD. (D) Schematic of *PDC1* premature stop codon (sc) and stem loop (sl) insertion. (E) *z*-stacked images of cells expressing Dcp2p-CFP and *PDC1-MS2* tagged mRNA. *PDC1-MS2* (sc) harbours a premature stop codon in the ORF. (F) *z*-stacked images of strains expressing Dcp2p-CFP and p*PDC1-MS2* or p*PDC1-MS2* (sl). p*PDC1-MS2* possesses a stem loop upstream of the ORF. (G) Scatter dotplot of mRNA granules per cell in *PDC1-MS2* tagged mRNA with or without a premature stop codon and in strains bearing p*PDC1-MS2* with or without the stem loop. Error bars are ± SD. Scale bars: 2μm (H) Relative fold change of (i) *PDC1 MS2*-tagged mRNA relative to untagged *PDC1* mRNA, (ii) *PDC1-MS2* mRNA in strains harbouring a premature stop codon (sc) relative to a strain without, (iii) *PDC1-*

MS2 mRNA on a plasmid (p*PDC1-MS2* mRNA) relative to genomic *PDC1-MS2* mRNA and finally (iv) p*PDC1*-MS2 mRNA in strain with a stem loop upstream of the ORF relative to a p*PDC1-MS2* mRNA without a stem loop. Error bars are ± SD.

Figure 6. CoFe granule number varies with quality of carbon source.

(A) *z*-stacked images of *PDC1-MS2* or *ENO1-MS2* mRNA in strains, co-expressing the MS2-CP-GFP fusion, grown in SC media supplemented with either 2% glucose, 2% raffinose, 2% galactose or 3% ethanol. Scale bar: 2μm. (B) Quantification of mRNA granules per cell for *PDC1* and *ENO1* mRNA in strains grown in the different carbon sources. n=50. Error bars are ± SD (C) Graph representing the relative fold change of *PDC1* or *ENO1* in strains grown in the different carbon source. Error bars are ± SD.

Figure 7. Human glycolytic mRNAs are present in granules and can colocalize.

(A) Scatter plot of particles detected from *z*-stacked images of Hela cells stained by smFISH for the mRNAs indicated. Images from 3 biological replicates were analyzed using the Image J ComDet plugin. Particle size is measured in pixels where each pixel = 45x45 nm. (B) Single *z*-slice images of HeLa cells stained by smFISH for the mRNAs indicated. Scale bar: 10μm. Insets show areas of interest magnified x2. (C) Histogram showing the percentage of colocalized mRNA particles calculated using ComDet analysis of *z*-slices from 3 biological replicates. The significance across the various combinations was calculated using one-way ANOVA. *ENO2* v *PFKM* (P value < 0.05 shown by asterisk) is significantly different to *ENO2* v *ENO1*, *ENO1* v *PFKM* or *ENO2* v *LDHA*.

Figure S1

(A) Graph representing the relative fold change of *MS2*-tagged mRNAs relative to untagged mRNA levels. Error bars represent ± SE. (B) *z*-stacked epifluorescent images of *ENO1* and *PFK2* mRNA harbouring 5 MS2 stem loops co-expressing the MS2-CP-GFP fusion. Scale bar: 2 μm (C) Northern blots of *ENO2* and *PDC1* mRNA in glucose replete and starved conditions in untagged strains or strains bearing the *MS2* tag.

Acknowledgements

We thank L. Berchowitz, J. Gerst, J. Chao and R. Singer for plasmid reagents and strains. Thanks go to Peter March and Steve Marsden for their help with the microscopy. FMP was supported by a CONICYT Becas Chile PhD studentship (ref. 72140307). CB and MP were supported by Wellcome Trust PhD studentships (210002/Z/17/Z and 099732/Z/12/Z). JL, CG and GF were supported by a Biotechnology and Biological Sciences Research Council (BBSRC) project grant (BB/K005979/1). JC was supported a BBSRC project grant (BB/P018270/1). The Bioimaging Facility microscopes used in this study were purchased with grants from BBSRC, Wellcome Trust and the University of Manchester Strategic Fund.

Author contributions

All authors generated reagents, performed experiments, evaluated results and generated figures. FMP, CB, JL, JC, MPA conceived the study, proposed and designed experiments, while MPA wrote the manuscript. All authors contributed to the discussion and evaluation of the manuscript.

References

Araiza-Olivera, D., Chiquete-Felix, N., Rosas-Lemus, M., Sampedro, J.G., Pena, A., Mujica, A., and Uribe-Carvajal, S. (2013). A glycolytic metabolon in Saccharomyces cerevisiae is stabilized by F-actin. FEBS J *280*, 3887-3905.

Ashe, M.P., De Long, S.K., and Sachs, A.B. (2000). Glucose depletion rapidly inhibits translation initiation in yeast. Mol Biol Cell *11*, 833-848.

Bar-Even, A., Flamholz, A., Noor, E., and Milo, R. (2012). Rethinking glycolysis: on the biochemical logic of metabolic pathways. Nat Chem Biol *8*, 509-517.

Barnett, J.A. (1976). The utilization of sugars by yeasts. Adv Carbohyd Chem Bi. *32*, 125-234.

Barnett, J.A. (2005). Glucose Catabolism in Yeast and Muscle. In Selected topics in the history of biochemistry: personal recollections, IX. volume editors Giorgio Semenza, A. J. Turner. In (Amsterdam ; London: Elsevier).

Benanti, J.A., Cheung, S.K., Brady, M.C., and Toczyski, D.P. (2007). A proteomic screen reveals SCFGrr1 targets that regulate the glycolytic-gluconeogenic switch. Nat Cell Biol *9*, 1184-1191.

Berleth, T., Burri, M., Thoma, G., Bopp, D., Richstein, S., Frigerio, G., Noll, M., and Nusslein-Volhard, C. (1988). The role of localization of bicoid RNA in organizing the anterior pattern of the Drosophila embryo. EMBO J *7*, 1749-1756.

Besse, F., and Ephrussi, A. (2008). Translational control of localized mRNAs: restricting protein synthesis in space and time. Nat Rev Mol Cell Biol *9*, 971-980.

Boukouris, A.E., Zervopoulos, S.D., and Michelakis, E.D. (2016). Metabolic Enzymes Moonlighting in the Nucleus: Metabolic Regulation of Gene Transcription. Trends Biochem Sci *41*, 712-730.

Brangwynne, C.P., Mitchison, T.J., and Hyman, A.A. (2011). Active liquid-like behavior of nucleoli determines their size and shape in Xenopus laevis oocytes. Proc Natl Acad Sci USA *108*, 4334-4339.

Campbell, S.G., Hoyle, N.P., and Ashe, M.P. (2005). Dynamic cycling of eIF2 through a large eIF2B-containing cytoplasmic body: implications for translation control. J Cell Biol *170*, 925-934.

Castello, A., Hentze, M.W., and Preiss, T. (2015). Metabolic Enzymes Enjoying New Partnerships as RNA-Binding Proteins. Trends Endocrinol Metab *26*, 746-757.

Chambers, A., Packham, E.A., and Graham, I.R. (1995). Control of glycolytic gene expression in the budding yeast (Saccharomyces cerevisiae). Curr Genet *29*, 1-9.

Daran-Lapujade, P., Rossell, S., van Gulik, W.M., Luttik, M.A., de Groot, M.J., Slijper, M., Heck, A.J., Daran, J.M., de Winde, J.H., Westerhoff, H.V.*, et al.* (2007). The fluxes through glycolytic enzymes in Saccharomyces cerevisiae are predominantly regulated at posttranscriptional levels. Proc Natl Acad Sci USA *104*, 15753-15758.

Decker, B.L., and Wickner, W.T. (2006). Enolase activates homotypic vacuole fusion and protein transport to the vacuole in yeast. J Biol Chem *281*, 14523-14528.

Diaz-Ruiz, R., Rigoulet, M., and Devin, A. (2011). The Warburg and Crabtree effects: On the origin of cancer cell energy metabolism and of yeast glucose repression. Biochim Biophys Acta *1807*, 568-576.

Duncan, C.D., and Mata, J. (2011). Widespread cotranslational formation of protein complexes. PLoS Genet *7*, e1002398.

Eliscovich, C., Shenoy, S.M., and Singer, R.H. (2017). Imaging mRNA and protein interactions within neurons. Proc Natl Acad Sci USA *114*, E1875-E1884.

Entelis, N., Brandina, I., Kamenski, P., Krasheninnikov, I.A., Martin, R.P., and Tarassov, I. (2006). A glycolytic enzyme, enolase, is recruited as a cofactor of tRNA targeting toward mitochondria in Saccharomyces cerevisiae. Genes Dev *20*, 1609-1620.

Gadir, N., Haim-Vilmovsky, L., Kraut-Cohen, J., and Gerst, J.E. (2011). Localization of mRNAs coding for mitochondrial proteins in the yeast Saccharomyces cerevisiae. RNA *17*, 1551-1565.

Garcia, J.F., and Parker, R. (2015). MS2 coat proteins bound to yeast mRNAs block 5' to 3' degradation and trap mRNA decay products: implications for the localization of mRNAs by MS2-MCP system. RNA *21*, 1393-1395.

Garcia, J.F., and Parker, R. (2016). Ubiquitous accumulation of 3' mRNA decay fragments in Saccharomyces cerevisiae mRNAs with chromosomally integrated MS2 arrays. RNA *22*, 657-659.

Gibson, D.G., Young, L., Chuang, R.Y., Venter, J.C., Hutchison, C.A., 3rd, and Smith, H.O. (2009). Enzymatic assembly of DNA molecules up to several hundred kilobases. Nat Methods *6*, 343-345.

Gill, K.S., Fernandes, P., O'Donovan, T.R., McKenna, S.L., Doddakula, K.K., Power, D.G., Soden, D.M., and Forde, P.F. (2016). Glycolysis inhibition as a cancer treatment and its role in an anti-tumour immune response. Biochim Biophys Acta *1866*, 87-105.

Haanstra, J.R., Gonzalez-Marcano, E.B., Gualdron-Lopez, M., and Michels, P.A. (2016). Biogenesis, maintenance and dynamics of glycosomes in trypanosomatid parasites. Biochim Biophys Acta *1863*, 1038-1048.

Hagan, K.W., Ruiz-Echevarria, M.J., Quan, Y., and Peltz, S.W. (1995). Characterization of cis-acting sequences and decay intermediates involved in nonsense-mediated mRNA turnover. Mol Cell Biol *15*, 809-823.

Haim-Vilmovsky, L., and Gerst, J.E. (2011). Visualizing endogenous mRNAs in living yeast using m-TAG, a PCR-based RNA aptamer integration method, and fluorescence microscopy. Methods Mol Biol *714*, 237-247.

Haimovich, G., Zabezhinsky, D., Haas, B., Slobodin, B., Purushothaman, P., Fan, L., Levin, J.Z., Nusbaum, C., and Gerst, J.E. (2016). Use of the MS2 aptamer and coat protein for RNA localization in yeast: A response to "MS2 coat proteins bound to yeast mRNAs block 5' to 3' degradation and trap mRNA decay products: implications for the localization of mRNAs by MS2-MCP system". RNA *22*, 660-666.

Halbach, A., Zhang, H., Wengi, A., Jablonska, Z., Gruber, I.M., Halbeisen, R.E., Dehe, P.M., Kemmeren, P., Holstege, F., Geli, V.*, et al.* (2009). Cotranslational assembly of the yeast SET1C histone methyltransferase complex. EMBO J *28*, 2959-2970.

Halstead, J.M., Lionnet, T., Wilbertz, J.H., Wippich, F., Ephrussi, A., Singer, R.H., and Chao, J.A. (2015). Translation. An RNA biosensor for imaging the first round of translation from single cells to living animals. Science *347*, 1367-1671.

Heinrich, S., Sidler, C.L., Azzalin, C.M., and Weis, K. (2017). Stem-loop RNA labeling can affect nuclear and cytoplasmic mRNA processing. RNA *23*, 134-141.

Herbert, A.D., Carr, A.M., and Hoffmann, E. (2014). FindFoci: a focus detection algorithm with automated parameter training that closely matches human assignments, reduces human inconsistencies and increases speed of analysis. PLoS One *9*, e114749.

Hocine, S., Raymond, P., Zenklusen, D., Chao, J.A., and Singer, R.H. (2013). Single-molecule analysis of gene expression using two-color RNA labeling in live yeast. Nat Methods *10*, 119-121.

Hoyle, N.P., and Ashe, M.P. (2008). Subcellular localization of mRNA and factors involved in translation initiation. Biochem Soc Trans *36*, 648-652.

Hubstenberger, A., Courel, M., Benard, M., Souquere, S., Ernoult-Lange, M., Chouaib, R., Yi, Z., Morlot, J.B., Munier, A., Fradet, M.*, et al.* (2017). P-Body Purification Reveals the Condensation of Repressed mRNA Regulons. Mol Cell *68*, 144-157 e145.

Jain, S., and Parker, R. (2013). The discovery and analysis of P Bodies. Adv Exp Med Biol *768*, 23-43.

Jin, M., Fuller, G.G., Han, T., Yao, Y., Alessi, A.F., Freeberg, M.A., Roach, N.P., Moresco, J.J., Karnovsky, A., *et al.* (2017 Glycolytic Enzymes Coalesce in G Bodies under Hypoxic Stress. Cell Rep. *25*, 895-908.

Jurica, M.S., Mesecar, A., Heath, P.J., Shi, W., Nowak, T., and Stoddard, B.L. (1998). The allosteric regulation of pyruvate kinase by fructose-1,6-bisphosphate. Structure *6*, 195-210.

Kamenova, I., Mukherjee, P., Conic, S., Mueller, F., El-Saafin, F., Bardot, P., Garnier, J.M., Dembele, D., Capponi, S., Timmers, H.T.M.*, et al.* (2019). Co-translational assembly of mammalian nuclear multisubunit complexes. Nat Commun *10*, 1740.

Kim, J.W., and Dang, C.V. (2005). Multifaceted roles of glycolytic enzymes. Trends Biochem Sci *30*, 142-150.

Knull, H.R., and Walsh, J.L. (1992). Association of glycolytic enzymes with the cytoskeleton. Curr Top Cell Reg *33*, 15-30.

Kojima, T., and Takayama, S. (2018). Membraneless Compartmentalization Facilitates Enzymatic Cascade Reactions and Reduces Substrate Inhibition. ACS Appl Mater Interfaces *10*, 32782-32791.

Krieger, K., and Ernst, J.F. (1994). Iron regulation of triosephosphate isomerase transcript stability in the yeast Saccharomyces cerevisiae. Microbiology *140 (Pt 5)*, 1079-1084.

Lecuyer, E., Yoshida, H., Parthasarathy, N., Alm, C., Babak, T., Cerovina, T., Hughes, T.R., Tomancak, P., and Krause, H.M. (2007). Global analysis of mRNA localization reveals a prominent role in organizing cellular architecture and function. Cell *131*, 174-187.

Lee, M., and Yoon, J.H. (2015). Metabolic interplay between glycolysis and mitochondrial oxidation: The reverse Warburg effect and its therapeutic implication. World J Biol Chem *6*, 148-161.

Lim, J.H., and Jung, G.Y. (2017). A simple method to control glycolytic flux for the design of an optimal cell factory. Biotechnol Biofuels *10*, 160.

Livak, K.J., and Schmittgen, T.D. (2001). Analysis of relative gene expression data using real-time quantitative PCR and the 2(-Delta Delta C(T)) Method. Methods *25*, 402-408.

Long, R.M., Singer, R.H., Meng, X., Gonzalez, I., Nasmyth, K., and Jansen, R.P. (1997). Mating type switching in yeast controlled by asymmetric localization of ASH1 mRNA. Science *277*, 383-387.

Lu, M., Ammar, D., Ives, H., Albrecht, F., and Gluck, S.L. (2007). Physical interaction between aldolase and vacuolar H+-ATPase is essential for the assembly and activity of the proton pump. J Biol Chem *282*, 24495-24503.

Lu, W., Zhang, Y., McDonald, D.O., Jing, H., Carroll, B., Robertson, N., Zhang, Q., Griffin, H., Sanderson, S., Lakey, J.H., *et al.* (2014). Dual proteolytic pathways govern glycolysis and immune competence. Cell *159*, 1578-1590.

Lui, J., Castelli, L.M., Pizzinga, M., Simpson, C.E., Hoyle, N.P., Bailey, K.L., Campbell, S.G., and Ashe, M.P. (2014). Granules harboring translationally active mRNAs provide a platform for P-body formation following stress. Cell Rep *9*, 944-954.

Lunghi, M., Galizi, R., Magini, A., Carruthers, V.B., and Di Cristina, M. (2015). Expression of the glycolytic enzymes enolase and lactate dehydrogenase during the early phase of Toxoplasma differentiation is regulated by an intron retention mechanism. Mol Microbiol *96*, 1159-1175.

Lunt, S.Y., and Vander Heiden, M.G. (2011). Aerobic glycolysis: meeting the metabolic requirements of cell proliferation. Annu Rev Cell Dev Biol *27*, 441-464.

Man, O., and Pilpel, Y. (2007). Differential translation efficiency of orthologous genes is involved in phenotypic divergence of yeast species. Nat Genet *39*, 415-421.

Masters, C. (1991). Cellular differentiation and the microcompartmentation of glycolysis. Mech Ageing Dev *61*, 11-22.

Masters, C.J., Reid, S., and Don, M. (1987). Glycolysis--new concepts in an old pathway. Mol Cell Biochem *76*, 3-14.

Matia-Gonzalez, A.M., Laing, E.E., and Gerber, A.P. (2015). Conserved mRNA-binding proteomes in eukaryotic organisms. Nat Struct Mol Biol *22*, 1027-1033.

Melton, D.A. (1987). Translocation of a localized maternal mRNA to the vegetal pole of Xenopus oocytes. Nature *328*, 80-82.

Miyashiro, K., Dichter, M., and Eberwine, J. (1994). On the nature and differential distribution of mRNAs in hippocampal neurites: implications for neuronal functioning. Proc Natl Acad Sci USA *91*, 10800-10804.

Mueller, F., Senecal, A., Tantale, K., Marie-Nelly, H., Ly, N., Collin, O., Basyuk, E., Bertrand, E., Darzacq, X., and Zimmer, C. (2013). FISH-quant: automatic counting of transcripts in 3D FISH images. Nat Methods *10*, 277-278.

Mugridge, J.S., Coller, J., and Gross, J.D. (2018). Structural and molecular mechanisms for the control of eukaryotic 5'-3' mRNA decay. Nat Struct Mol Biol *25*, 1077-1085.

Nelson, D.L., and Cox, M.M. (2017) Lehninger principles of biochemistry, Seventh edition. W.H. Freeman, New York, 1328.

Ngo, H., Tortorella, S.M., Ververis, K., and Karagiannis, T.C. (2015). The Warburg effect: molecular aspects and therapeutic possibilities. Mol Biol Rep *42*, 825-834.

Oparina, N.Y., Snezhkina, A.V., Sadritdinova, A.F., Veselovskii, V.A., Dmitriev, A.A., Senchenko, V.N., Mel'nikova, N.V., Speranskaya, A.S., Darii, M.V., Stepanov, O.A., *et al.* (2013). Differential expression of genes that encode glycolysis enzymes in kidney and lung cancer in humans. Genetika *49*, 814-823.

Palam, L.R., Baird, T.D., and Wek, R.C. (2011). Phosphorylation of eIF2 facilitates ribosomal bypass of an inhibitory upstream ORF to enhance CHOP translation. J Biological Chem *286*, 10939-10949.

Pfaffl, M.W. (2001). A new mathematical model for relative quantification in real-time RT-PCR. Nucleic Acids Res *29*, e45.

Pizzinga, M., and Ashe, M.P. (2014). Yeast mRNA localization: protein asymmetry, organelle localization and response to stress. Biochem Soc Trans *42*, 1256-1260.

Pizzinga, M., Bates, C., Lui, J., Forte, G., Morales-Polanco, F., Linney, E., Knotkova, B., Wilson, B., Solari, C.A., Berchowitz, L.E., *et al.* (2019). Translation factor mRNA granules direct protein synthetic capacity to regions of polarized growth. J Cell Biol *218*, 1564-1581.

Postmus, J., Aardema, R., de Koning, L.J., de Koster, C.G., Brul, S., and Smits, G.J. (2012). Isoenzyme expression changes in response to high temperature determine the metabolic regulation of increased glycolytic flux in yeast. FEMS Yeast Res *12*, 571-581.

Puchulu-Campanella, E., Chu, H., Anstee, D.J., Galan, J.A., Tao, W.A., and Low, P.S. (2013). Identification of the components of a glycolytic enzyme metabolon on the human red blood cell membrane. J Biol Chem *288*, 848-858.

Ray, L.B. (2010). Metabolism. Metabolism is not boring. Introduction. Science *330*, 1337.

Riera, L., Obach, M., Navarro-Sabate, A., Duran, J., Perales, J.C., Vinals, F., Rosa, J.L., Ventura, F., and Bartrons, R. (2003). Regulation of ubiquitous 6-phosphofructo-2-kinase by the ubiquitin-proteasome proteolytic pathway during myogenic C2C12 cell differentiation. FEBS Lett *550*, 23-29.

Rigden, D.J., Alexeev, D., Phillips, S.E., and Fothergill-Gilmore, L.A. (1998). The 2.3 A X-ray crystal structure of S. cerevisiae phosphoglycerate mutase. J Mol Biol *276*, 449-459.

Roy, B., and Jacobson, A. (2013). The intimate relationships of mRNA decay and translation. Trends Genet *29*, 691-699.

Schurr, A., and Gozal, E. (2015). Glycolysis at 75: is it time to tweak the first elucidated metabolic pathway in history? Front Neurosci *9*, 170.

Schwock, J., Kirchberger, J., Edelmann, A., Kriegel, T.M., and Kopperschlager, G. (2004). Interaction of 6-phosphofructokinase with cytosolic proteins of Saccharomyces cerevisiae. Yeast *21*, 483-494.

Shen, Q., Wang, G., Li, S., Liu, X., Lu, S., Chen, Z., Song, K., Yan, J., Geng, L., Huang, Z., *et al.* (2016). ASD v3.0: unraveling allosteric regulation with structural mechanisms and biological networks. Nucleic Acids Res *44*, D527-535.

Shenton, D., and Grant, C.M. (2003). Protein S-thiolation targets glycolysis and protein synthesis in response to oxidative stress in the yeast Saccharomyces cerevisiae. Biochem J *374*, 513-519.

Shiber, A., Doring, K., Friedrich, U., Klann, K., Merker, D., Zedan, M., Tippmann, F., Kramer, G., and Bukau, B. (2018). Cotranslational assembly of protein complexes in eukaryotes revealed by ribosome profiling. Nature *561*, 268-272.

Simpson, C.E., Lui, J., Kershaw, C.J., Sims, P.F., and Ashe, M.P. (2014). mRNA localization to P-bodies in yeast is bi-phasic with many mRNAs captured in a late Bfr1p-dependent wave. J Cell Sci *127*, 1254-1262.

Sims, P.A., Menefee, A.L., Larsen, T.M., Mansoorabadi, S.O., and Reed, G.H. (2006). Structure and catalytic properties of an engineered heterodimer of enolase composed of one active and one inactive subunit. J Mol Biol *355*, 422-431.

Timson, D.J. (2007). Galactose metabolism in Saccharomyces cerevisiae. Dyn Biochem Process Biotechnol Mol Biol *1*, 63-73.

Tripodi, F., Nicastro, R., Reghellin, V., and Coccetti, P. (2015). Post-translational modifications on yeast carbon metabolism: Regulatory mechanisms beyond transcriptional control. Biochim Biophys Acta *1850*, 620-627.

Tsanov, N., Samacoits, A., Chouaib, R., Traboulsi, A.M., Gostan, T., Weber, C., Zimmer, C., Zibara, K., Walter, T., Peter, M., *et al.* (2016). smiFISH and FISH-quant - a flexible single RNA detection approach with super-resolution capability. Nucleic Acids Res *44*, e165.

Vattem, K.M., and Wek, R.C. (2004). Reinitiation involving upstream ORFs regulates ATF4 mRNA translation in mammalian cells. Proc Natl Acad Sci USA *101*, 11269-11274.

Warmoes, M.O., and Locasale, J.W. (2014). Heterogeneity of glycolysis in cancers and therapeutic opportunities. Biochem Pharmacol *92*, 12-21.

Wegner, A., Meiser, J., Weindl, D., and Hiller, K. (2015). How metabolites modulate metabolic flux. Curr Opin Biotechnol *34*, 16-22.

Wells, J.N., Bergendahl, L.T., and Marsh, J.A. (2015). Co-translational assembly of protein complexes. Biochem Soc Trans *43*, 1221-1226.

Yeung, S.J., Pan, J., and Lee, M.H. (2008). Roles of p53, MYC and HIF-1 in regulating glycolysis - the seventh hallmark of cancer. Cell Mol Life Sci *65*, 3981-3999.

Zhou, H.X., Rivas, G., and Minton, A.P. (2008). Macromolecular crowding and confinement: biochemical, biophysical, and potential physiological consequences. Ann Rev Biophys *37*, 375-397.

Zipor, G., Haim-Vilmovsky, L., Gelin-Licht, R., Gadir, N., Brocard, C., and Gerst, J.E. (2009). Localization of mRNAs coding for peroxisomal proteins in the yeast, Saccharomyces cerevisiae. Proc Natl Acad Sci USA *106*, 19848-19853.

Zivraj, K.H., Tung, Y.C., Piper, M., Gumy, L., Fawcett, J.W., Yeo, G.S., and Holt, C.E. (2010). Subcellular profiling reveals distinct and developmentally regulated repertoire of growth cone mRNAs. J Neurosci *30*, 15464-15478.

Zwicker, D., Decker, M., Jaensch, S., Hyman, A.A., and Julicher, F. (2014). Centrosomes are autocatalytic droplets of pericentriolar material organized by centrioles. Proc Natl Acad Sci USA *111*, E2636-2645.

Table I. Yeast strains used in this study

Strain name	Genotype	Source
yMK467	*MATα ADE2 his3-11,15 leu2-3,112 trp1-1 ura3-1*	Campbell et al., 2005
yMK807	*MATa ADE2 his3-11,15 leu2-3,112 trp1-1 ura3-1*	Campbell et al., 2005
yMK1577	yMK807 *ENO2-MS2L* p[*MS2-GFP$_3$ HIS3*]	Lui et al., 2014
yMK1586	yMK467 *PDC1-MS2L* p[*MS2-GFP$_3$ HIS3*]	Lui et al., 2014
yMK1651	yMK467 *PDC1-MS2L DCP2*-CFP p[*MS2-GFP$_3$ HIS3*]	Lui et al., 2014
yMK2257	yMK467 *ENO2-PP7L PDC1-MS2L* p[*MS2-mCh$_3$ HIS3*] p[*PP7-GFP$_2$ URA3*]	Lui et al., 2014
yMK2412	yMK467 *PFK1-MS2L* p[*MS2-GFP$_3$ HIS3*]	This study
yMK2413	yMK467 *PYK2-MS2L* p[*MS2- GFP$_3$ HIS3*]	This study
yMK2415	yMK467 *PFK2-MS2L* (5 loops) p[*MS2- GFP$_3$ HIS3*]	This study
yMK2416	yMK467 *FBA1-MS2L* p[*MS2- GFP$_3$ HIS3*]	This study
yMK2429	yMK467 p[*MS2-GFP$_3$ HIS3*]	This study
yMK2430	yMK467 *TPI1-MS2L* p[*MS2-GFP$_3$ HIS3*]	This study
yMK2431	yMK467 *GLK1-MS2L* p[*MS2-GFP$_3$ HIS3*]	This study
yMK2447	yMK467 *ADH1-MS2L* p[*MS2-GFP$_3$ HIS3*]	This study
yMK2452	yMK467 *PDC1-MS2L* (sc) *DCP2*-CFP p[*MS2-GFP$_3$ HIS3*]	This study
yMK2480	yMK467 *PFK2-MS2L* p[*MS2-GFP$_3$ HIS3*]	This study
yMK2535	yMK467 *PGK1-MS2L* p[*MS2- GFP$_3$ HIS3*]	This study
yMK2461	yMK467 *ENO1-MS2L* (5 loops) p[*MS2- GFP$_3$ HIS3*]	This study
yMK2468	yMK467 *ENO1-MS2L* p[*MS2- GFP$_3$ HIS3*]	This study
yMK2580	yMK467 *HXK1-MS2L* p[*MS2- GFP$_3$ HIS3*]	This study
yMK2582	yMK467 *CDC19-MS2L* p[*MS2- GFP$_3$ HIS3*]	This study
yMK2585	yMK467 *TDH3-MS2L* p[*MS2- GFP$_3$ HIS3*]	This study
yMK2588	yMK467 *GLO1-MS2L* p[*MS2- GFP$_3$ HIS3*]	This study
yMK2594	yMK467 *ENO2-PP7L PFK1-MS2L* p[*MS2-mCh$_3$ HIS3*] p[*PP7–GFP$_2$ URA3*]	This study
yMK2596	yMK467 *ENO2-PP7L PGI1-MS2L* p[*MS2-mCh$_3$ HIS3*] p[*PP7–GFP$_2$ URA3*]	This study
yMK2600	yMK467 *ENO2-PP7L ADH1-MS2L* p[*MS2-mCh$_3$ HIS3*] p[*PP7–GFP$_2$ URA3*]	This study
yMK2601	yMK467 *ENO2-PP7L CDC19-MS2L* p[*MS2-mCh$_3$ HIS3*] p[*PP7–GFP$_2$ URA3*]	This study
yMK2602	yMK467 *ENO2-PP7L TDH3-MS2L* p[*MS2-mCh$_3$ HIS3*] p[*PP7–GFP$_2$ URA3*]	This study
yMK2603	yMK467 *ENO2-PP7L PFK2-MS2L* p[*MS2-mCh$_3$ HIS3*] p[*PP7–GFP$_2$ URA3*]	This study
yMK2604	yMK467 *ENO2-PP7L TPI1-MS2L* p[*MS2-mCh$_3$ HIS3*] p[*PP7–GFP$_2$ URA3*]	This study
yMK2699	yMK467 *HXK2-MS2L* p[*MS2- GFP$_3$ HIS3*]	This study
yMK2700	yMK467 *PFK26-MS2L* p[*MS2- GFP$_3$ HIS3*]	This study
yMK2705	yMK467 *ENO2-PP7L GPM1-MS2L* p[*MS2 -mCh$_3$ HIS3*] p[*PP7 –GFP$_2$ URA3*]	This study
yMK2738	yMK467 *DCP2*-CFP p[*MS2- GFP$_3$ HIS3*] p[*PDC1-MS2-SL*]	This study
yMK3162	yMK807 *DCP2*-CFP p[*MS2- GFP$_3$ HIS3*] p[*PDC1-MS2*]	This study
yMK3176	yMK467 *GPM1-MS2L* p[*MS2- GFP$_3$ HIS3*]	This study
yMK3397	yMK467 *PGI1-MS2L* p[*MS2- GFP$_3$ HIS3*]	This study

Figure 1. Morales-Polanco et al

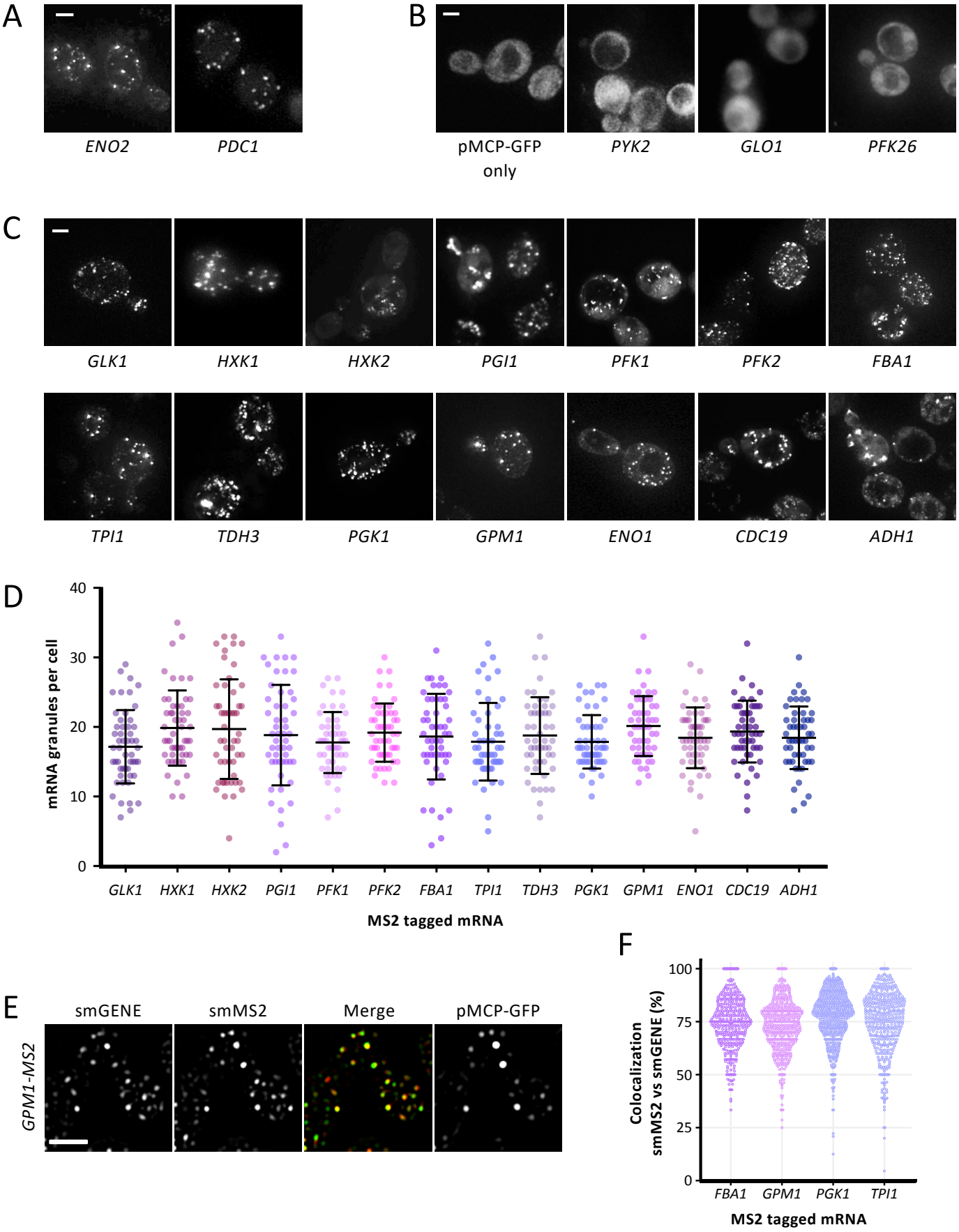

Figure 2. Morales-Polanco et al

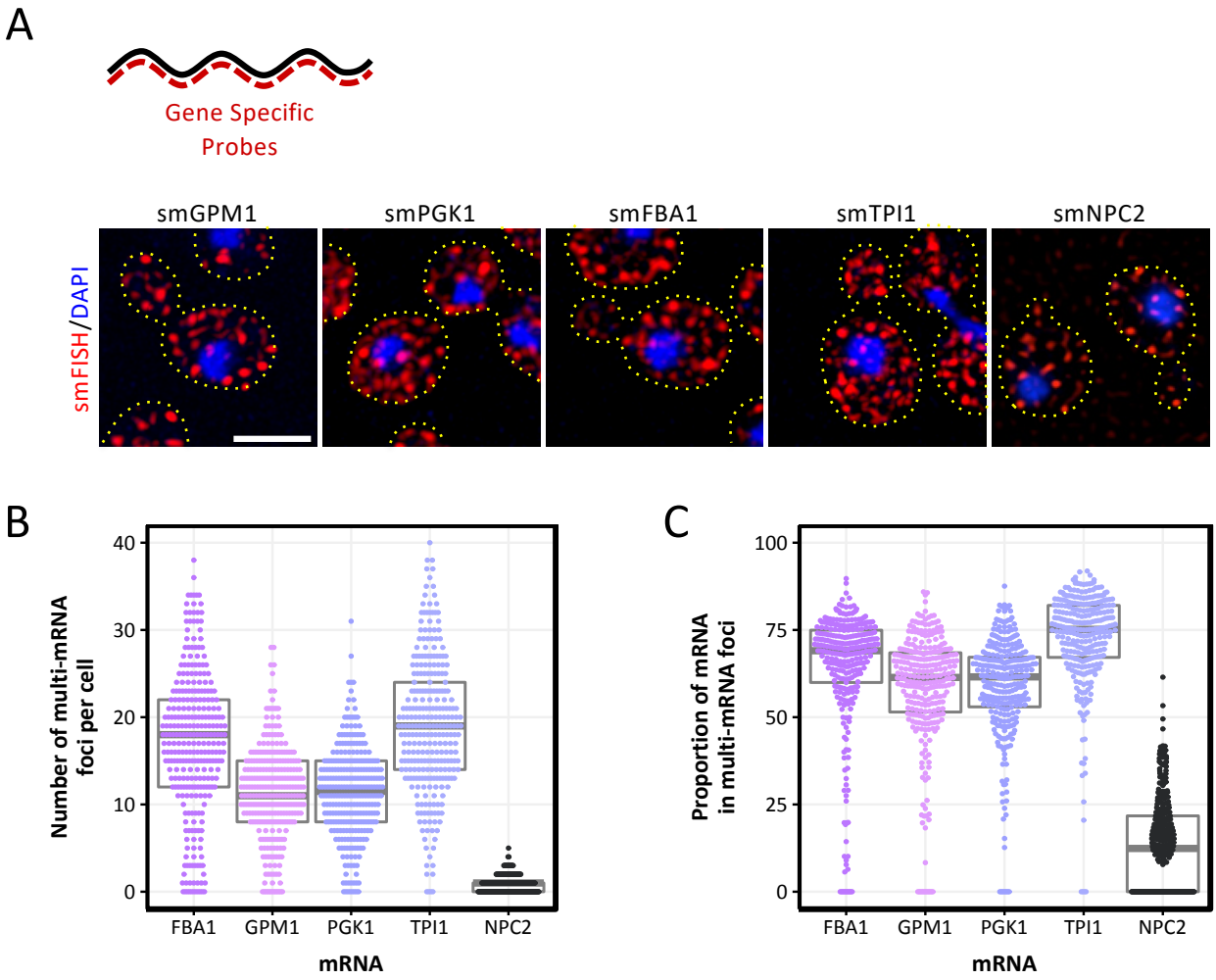

Figure 3. Morales-Polanco et al

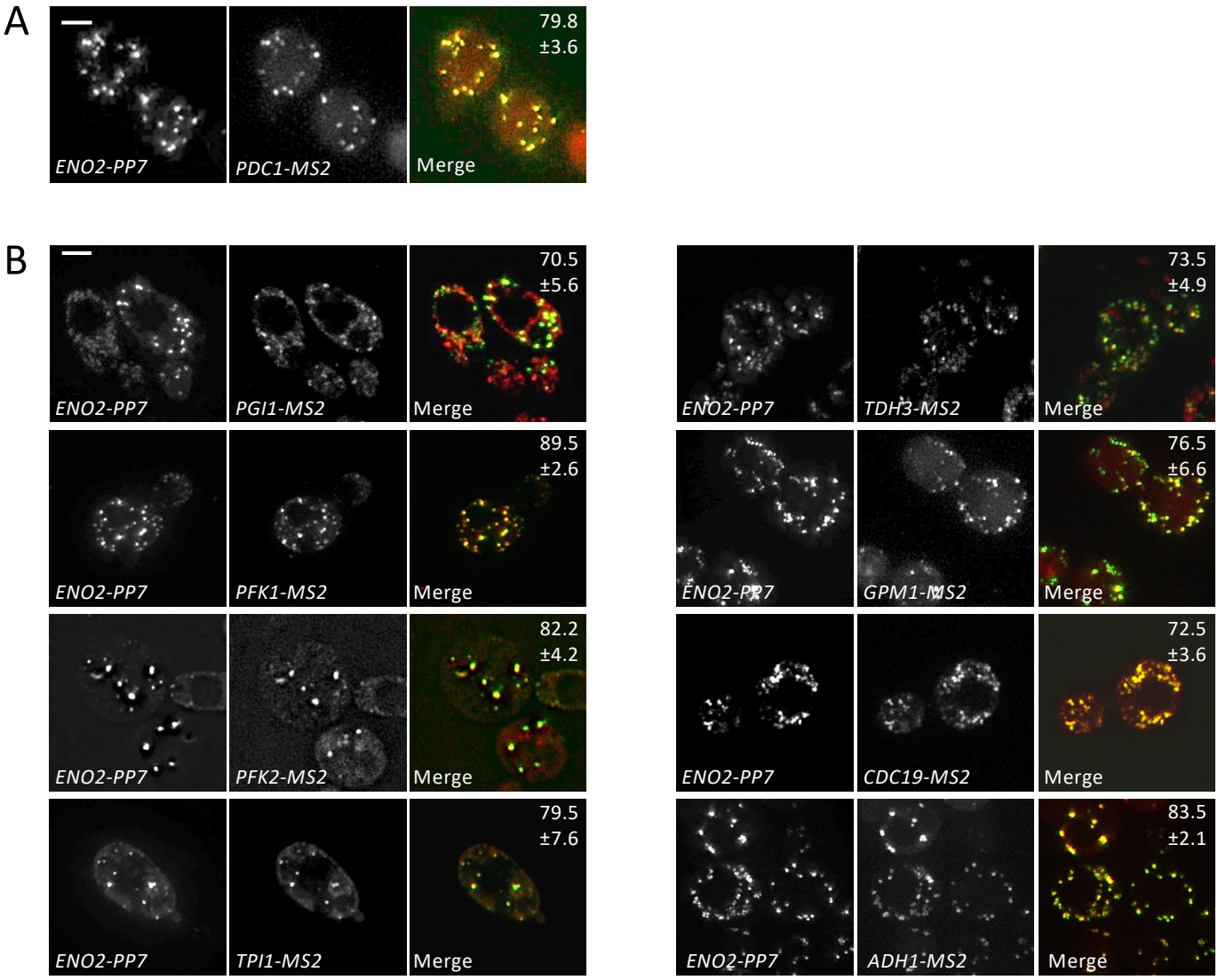

Figure 4. Morales-Polanco et al

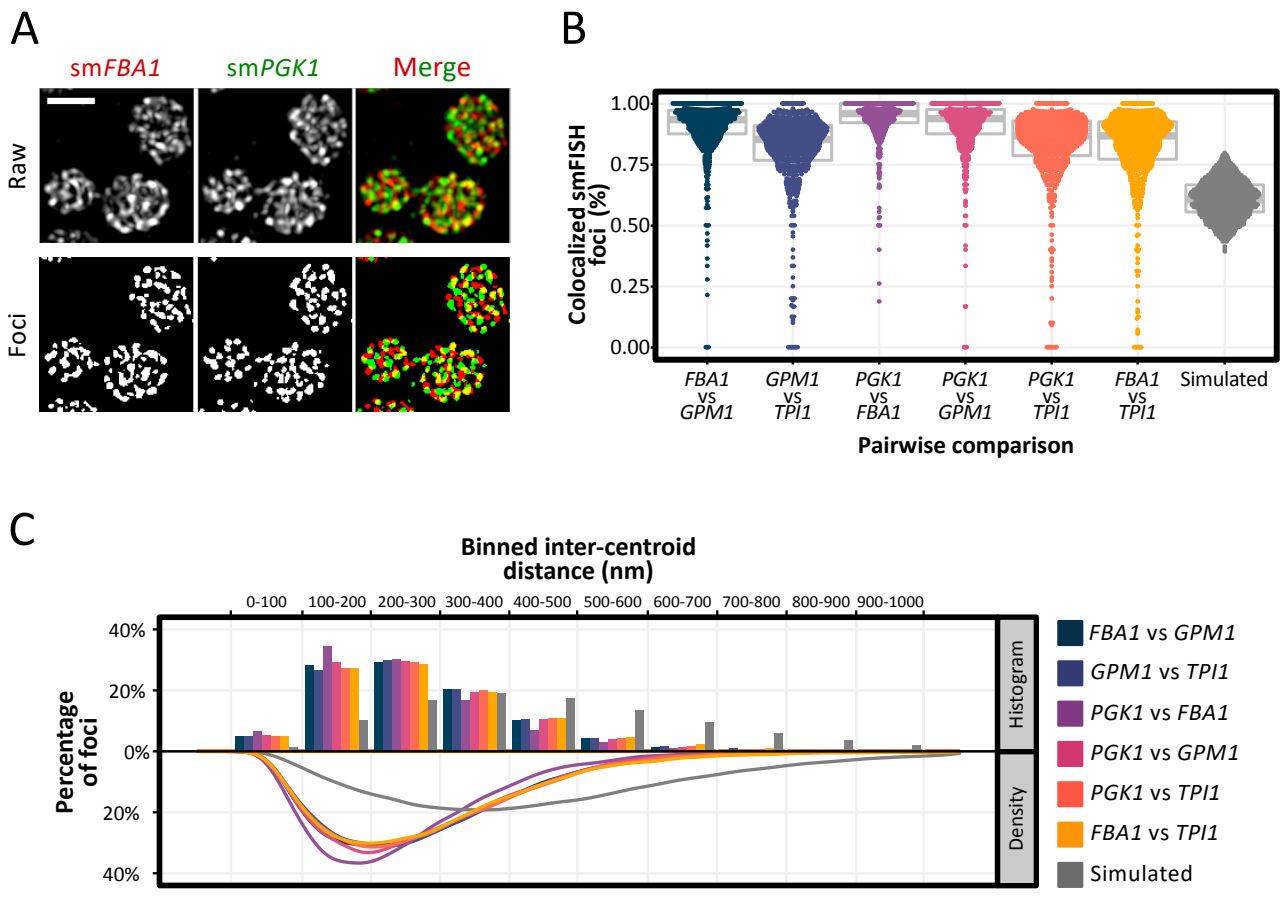

Figure 5. Morales-Polanco et al

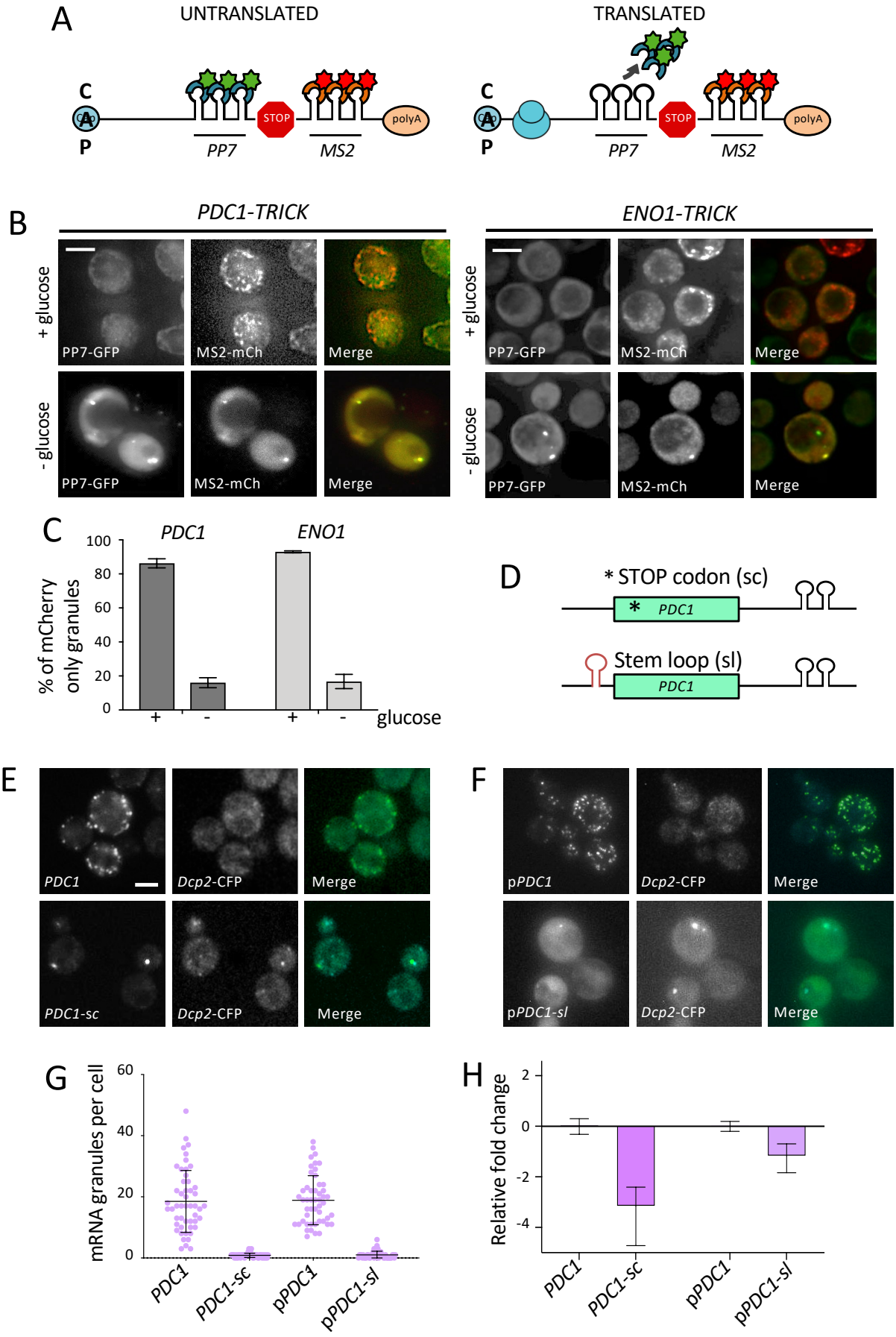

Figure 6. Morales-Polanco et al

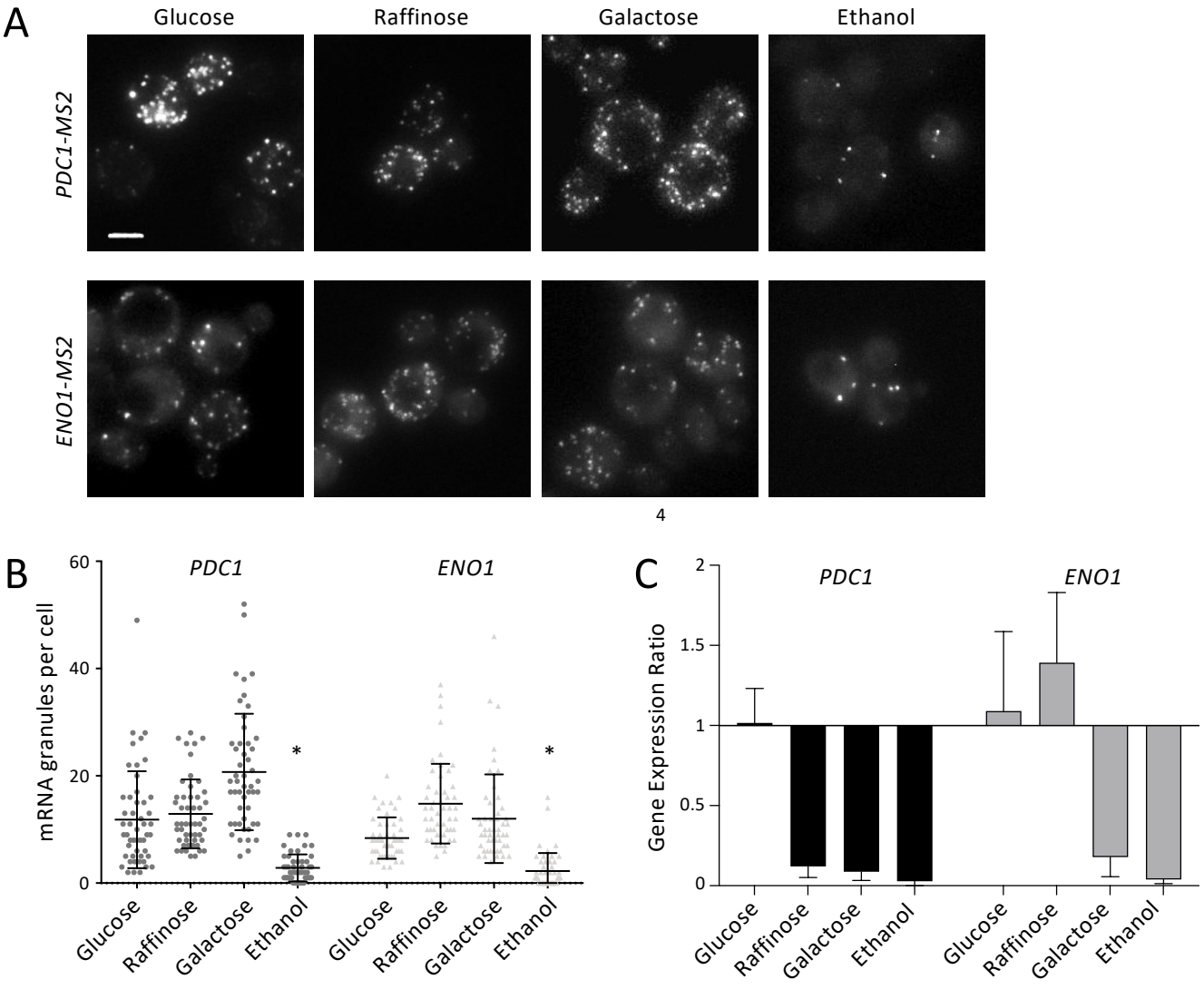

Figure 7. Morales-Polanco et al

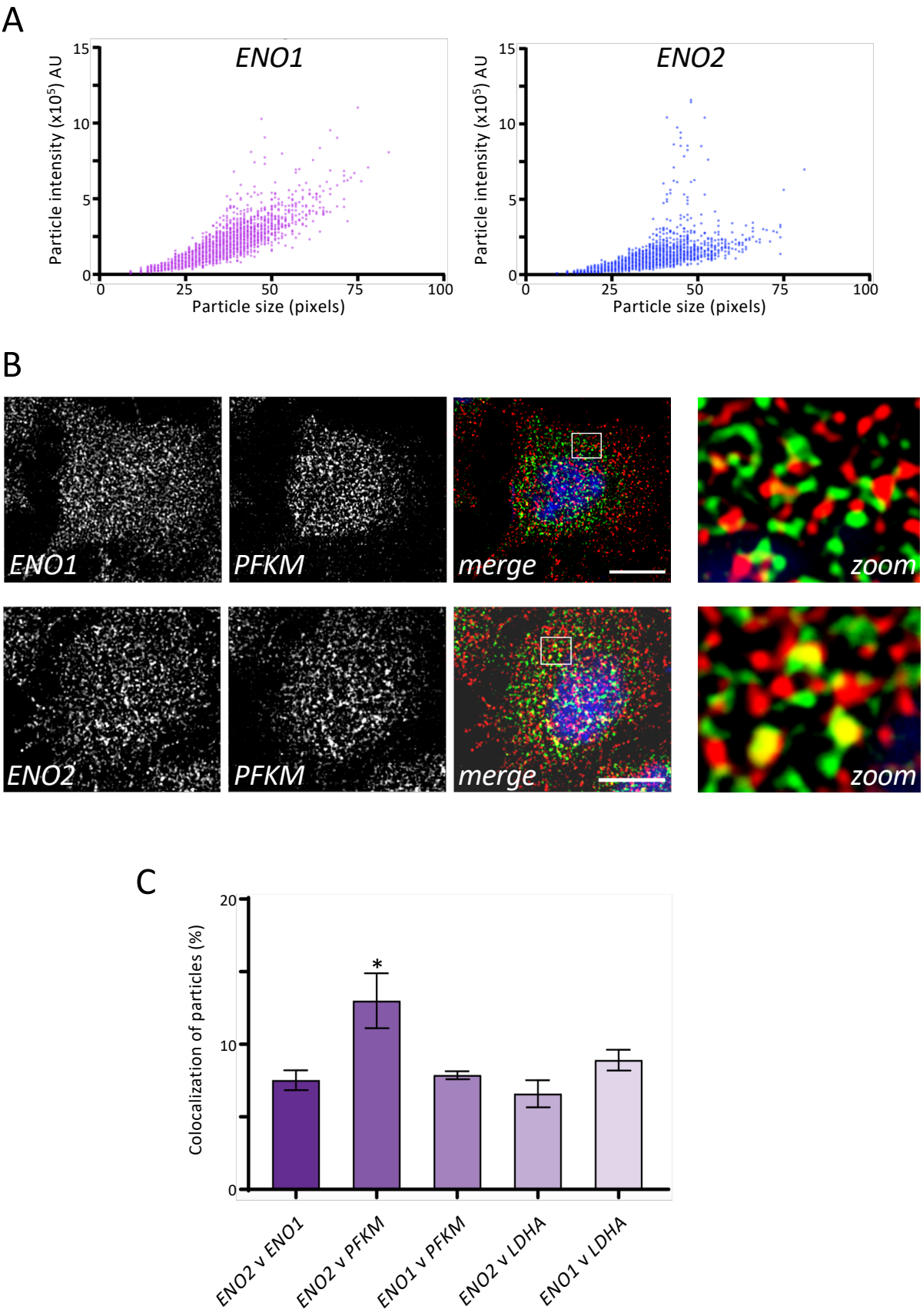

Supplementary figure 1. Morales-Polanco et al